**Structure, Volume *21***

## Supplemental Information

# Structure of HHARI, a RING-IBR-RING Ubiquitin Ligase: Autoinhibition of an Ariadne-Family E3 and Insights into Ligation Mechanism

**David M. Duda, Jennifer L. Olszewski, Jonathan P. Schuermann, Igor Kurinov, Darcie J. Miller, Amanda Nourse, Arno F. Alpi, and Brenda A. Schulman**

**Inventory of Supplemental Information**

**Item**

**SUPPLEMENTARY FIGURES**

**Supplementary Figure 1. Electron density over HHARI domains. [supports Figure 2]**

**Supplementary Figure 2. Packing in HHARI crystals and AUC and SEC-MALS data on HHARI. [supports Table 1]**

**Supplementary Figure 3. Sequence alignment of Ariadne family members and RBR E3s. [supports Figure 3]**

**Supplementary Figure 4. Analysis of HHARI UBA-like domain. [supports Figure 5]**

**SUPPLEMENTARY TABLE**

**Supplementary Table 1. Selected contacts between HHARI RING2 and Ariadne domains. [supports Figure 4]**

**SUPPLEMENTARY EXPERIMENTAL PROCEDURES**

**Protein expression and purification**

**Analytical Ultracentrifugation and SEC-MALS**

**SUPPLEMENTARY REFERENCES**

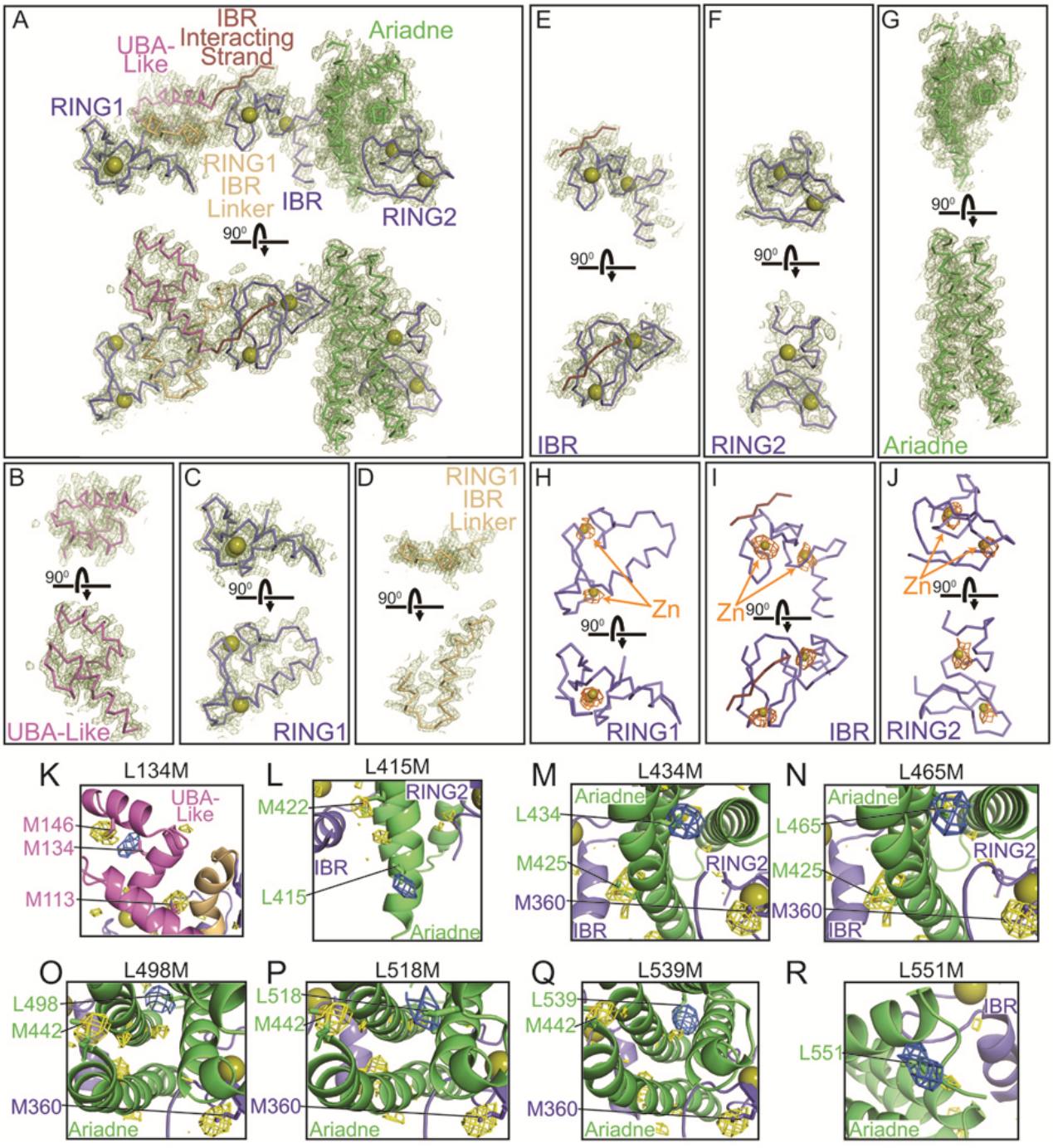
A
IBR
Interacting
Strand
UBA-
Like
Ariadne
RING1
RING1
IBR
Linker
IBR
RING2
90°
E
IBR
F
RING2
G
Ariadne
B
UBA-Like
C
RING1
D
RING1
IBR
Linker
H
Zn
RING1
I
Zn
IBR
J
Zn
RING2
K
L134M
UBA-
Like
M146
M134
M113
L
L415M
RING2
M422
IBR
L415
Ariadne
M
L434M
Ariadne
L434
M425
RING2
M360
IBR
N
L465M
Ariadne
L465
RING2
M425
M360
IBR
O
L498M
L498
M442
M360
Ariadne
P
L518M
L518
M442
M360
Ariadne
Q
L539M
L539
M442
M360
Ariadne
R
L551M
IBR
L551
Ariadne

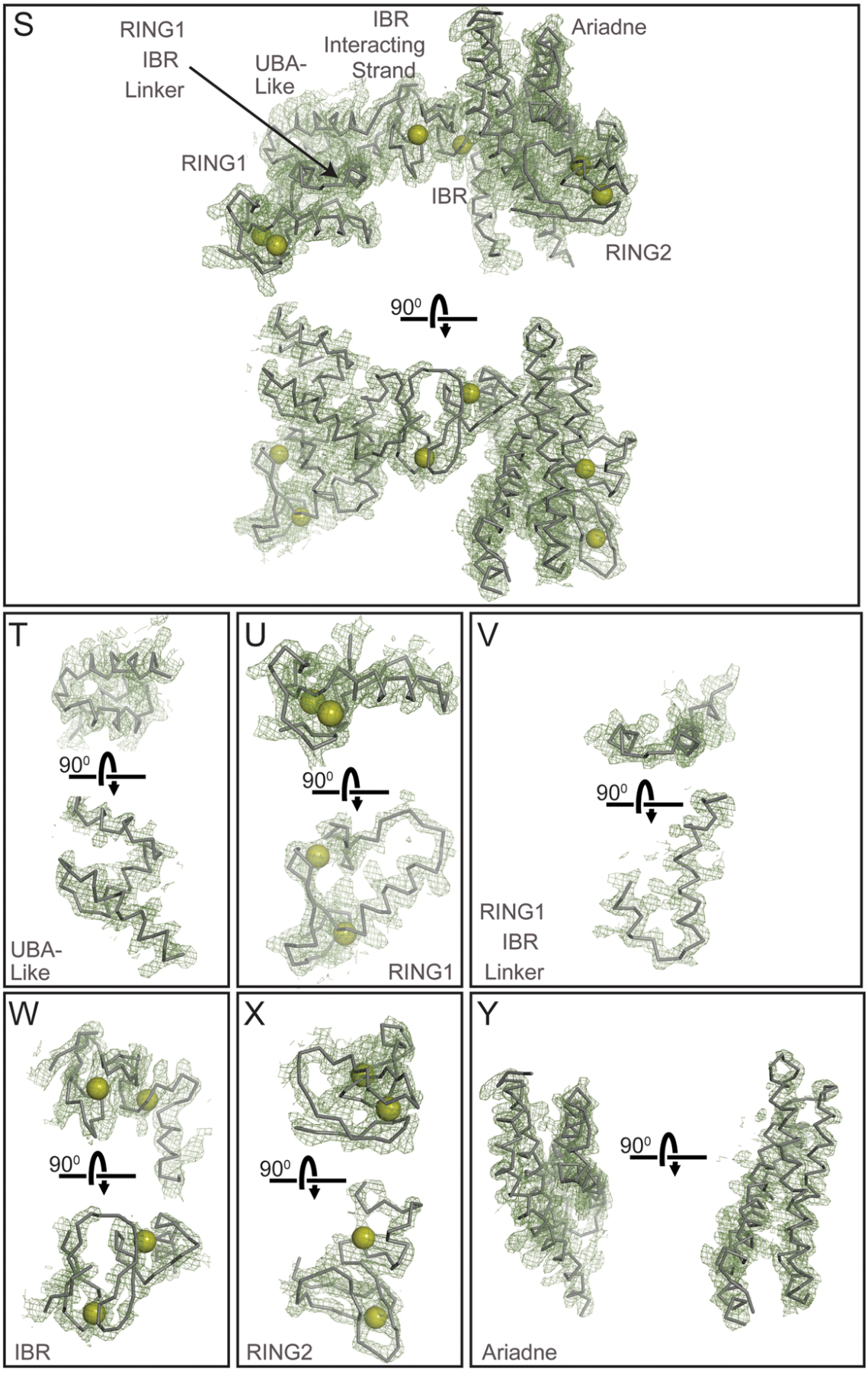
S
RING1
IBR
Linker
UBA-
Like
IBR
Interacting
Strand
Ariadne
RING1
IBR
RING2
90⁰
T
90⁰
UBA-
Like
U
90⁰
RING1
V
90⁰
RING1
IBR
Linker
W
90⁰
IBR
X
90⁰
RING2
Y
90⁰
Ariadne

**Figure S1. Electron density over HHARI domans. [supports Figure 2]**

A. Final 2Fo-Fc electron density of $P4_1$ HHARI crystal form contoured at 1.5σ.
B. Final 2Fo-Fc electron density over the UBA-like domain of HHARI $P4_1$ crystal form contoured at 1.5σ.
C. Final 2Fo-Fc electron density over RING1 of HHARI $P4_1$ crystal form contoured at 1.5σ.
D. Final 2Fo-Fc electron density over RING1-IBR-Linker of HHARI $P4_1$ crystal form contoured at 1.5σ.
E. Final 2Fo-Fc electron density over the IBR of HHARI $P4_1$ crystal form contoured at 1.5σ.
F. Final 2Fo-Fc electron density over RING2 of HHARI $P4_1$ crystal form contoured at 1.5σ.
G. Final 2Fo-Fc electron density over Ariadne domain of HHARI $P4_1$ crystal form contoured at 1.5σ.
H. Anomalous difference density contoured at 3σ from data collected at the zinc edge 1.28Å showing the position of the two zinc atoms in RING1.
I. Anomalous difference density contoured at 3σ from data collected at the zinc edge 1.28Å showing the position of the two zinc atoms in the IBR.
J. Anomalous difference density contoured at 3σ from data collected at the zinc edge 1.28Å showing the position of the two zinc atoms in RING2.
K. Anomalous difference density contoured at 3σ from data collected at the selenium edge 0.979Å showing the position of the engineered L134M mutation (blue density) used to guide structure building. Yellow density shows the positions of two natural methionines (M113 and M146).
L. Anomalous difference density contoured at 3σ from data collected at the selenium edge 0.979Å showing the position of the engineered L415M mutation (blue density) used to guide structure building. Yellow density shows the positions of the natural methionine M422.
M. Anomalous difference density contoured at 3σ from data collected at the selenium edge 0.979Å showing the position of the engineered L434M mutation (blue density) used to guide structure building. Yellow density shows the positions of two natural methionines (M360 and M425).
N. Anomalous difference density contoured at 3σ from data collected at the selenium edge 0.979Å showing the position of the engineered L465M mutation (blue density) used to guide structure building. Yellow density shows the positions of two natural methionines (M360 and M425).
O. Anomalous difference density contoured at 3σ from data collected at the selenium edge 0.979Å showing the position of the engineered L498M mutation (blue density) used to guide structure building. Yellow density shows the positions of two natural methionines (M360 and M442).
P. Anomalous difference density contoured at 3σ from data collected at the selenium edge 0.979Å showing the position of the engineered L518M mutation (blue density) used to guide structure building. Yellow density shows the positions of two natural methionines (M360 and M442).
Q. Anomalous difference density contoured at 3σ from data collected at the selenium edge 0.979Å showing the position of the engineered L539M mutation (blue density) used to guide structure building. Yellow density shows the positions of two natural methionines (M360 and M442).

R. Anomalous difference density contoured at 3σ from data collected at the selenium edge 0.979Å showing the position of the engineered L551M mutation (blue density) used to guide structure building.
S. Final 2Fo-Fc electron density of $P6_3$ HHARI crystal form contoured at 1.5σ.
T. Final 2Fo-Fc electron density over the UBA-like domain of HHARI $P6_3$ crystal form contoured at 1.5σ.
U. Final 2Fo-Fc electron density over RING1 of HHARI $P6_3$ crystal form contoured at 1.5σ.
V. Final 2Fo-Fc electron density over the RING1-IBR-Linker of HHARI $P6_3$ crystal form contoured at 1.5σ.
W. Final 2Fo-Fc electron density over the IBR of HHARI $P6_3$ crystal form contoured at 1.5σ.
X. Final 2Fo-Fc electron density over RING2 of HHARI $P6_3$ crystal form contoured at 1.5σ.
Y. Final 2Fo-Fc electron density over the Ariadne domain of HHARI $P6_3$ crystal form contoured at 1.5σ.

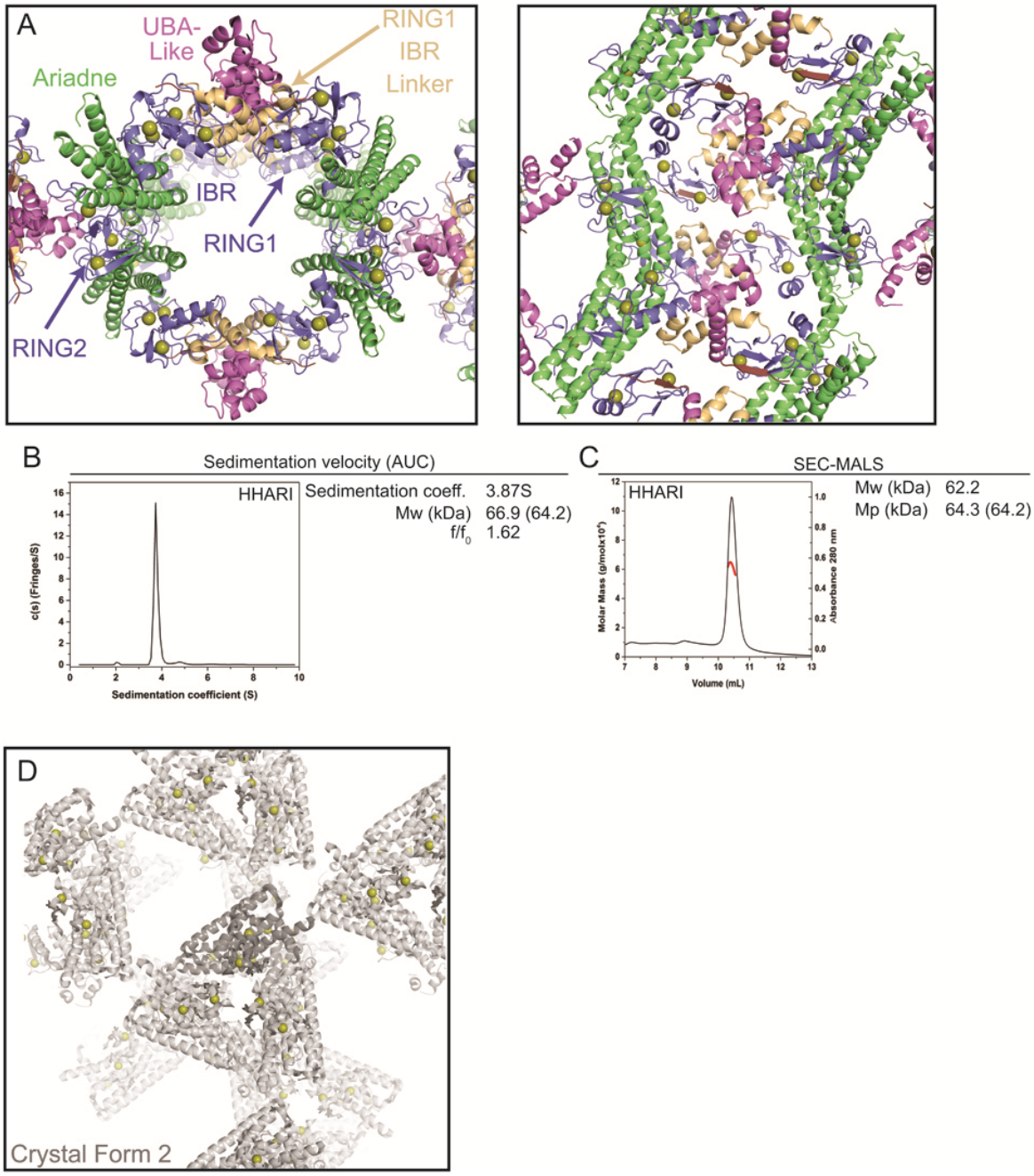


**Figure S2. Packing in HHARI crystals and AUC and SEC-MALS data on HHARI. [supports Table 1]**

A. Two views of crystal packing for the $P4_1$ crystal form of HHARI.
B. Sedimentation velocity AUC of HHARI showing a single peak from the sedimentation coefficient distribution *c(s)* analysis. The sedimentation coefficient, frictional ratio and molecular weight from the analysis are shown with theoretical value in parentheses.
C. SEC-MALS data for HHARI plotted as a molar mass distribution (red) superimposed on chromatogram of absorbance at 280 nm versus elution volume. Molecular weight (MW) determined by SEC-MALS is shown with theoretical value in parentheses.
D. Crystal packing of the $P6_3$ crystal form of HHARI.

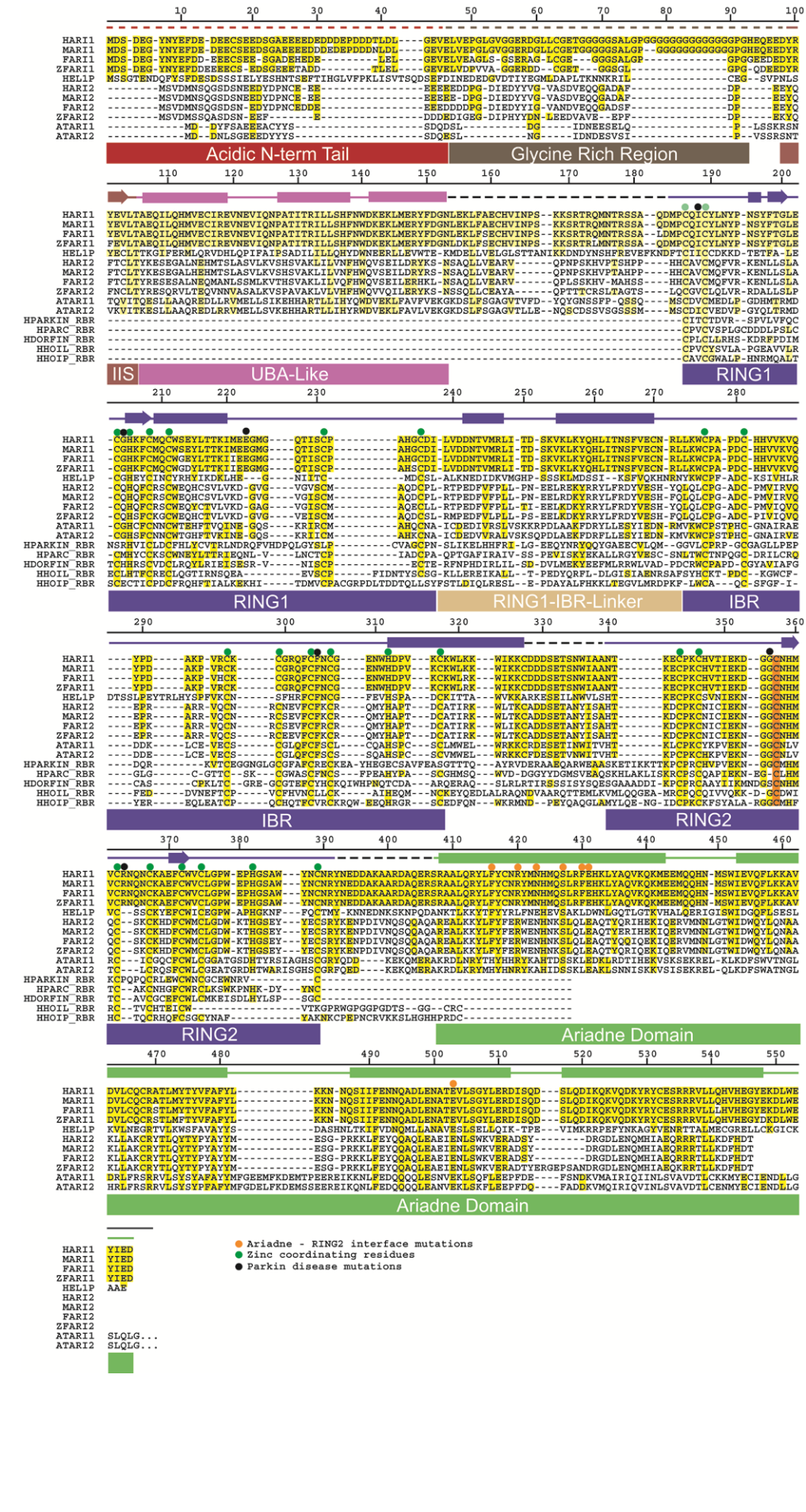
Acidic N-term Tail
Glycine Rich Region
IIS
UBA-Like
RING1
RING1
RING1-IBR-Linker
IBR
IBR
RING2
RING2
Ariadne Domain
Ariadne Domain
Ariadne - RING2 interface mutations
Zinc coordinating residues
Parkin disease mutations

**Figure S3. Sequence alignment of Ariadne family members and RBR E3s. [supports Figure 3]**

Alignment of HHARI (HARI1) with mouse, frog and zebrafish ARI1, as well as human, mouse, frog and zebrafish ARI2, yeast HEL1p, and the related RBR proteins Parkin, PARC, Dorfin, HOIL-1L and HOIP. Only the RBR region for Parkin, PARC, Dorfin, HOIL-1L and HOIP are displayed. Sequence numbering corresponds to HARI1. Secondary structure based on the structure of HARI1 is displayed underneath while domain architecture is shown above. Residues involved in zinc coordination are denoted with a green dot. Mutations that disrupt the RING2-Ariadne interface and are activating are denoted with an orange dot. Positions of common Parkin mutations associated with Autosomal Recessive Juvenile Parkinson's Disease are denoted with black dots.

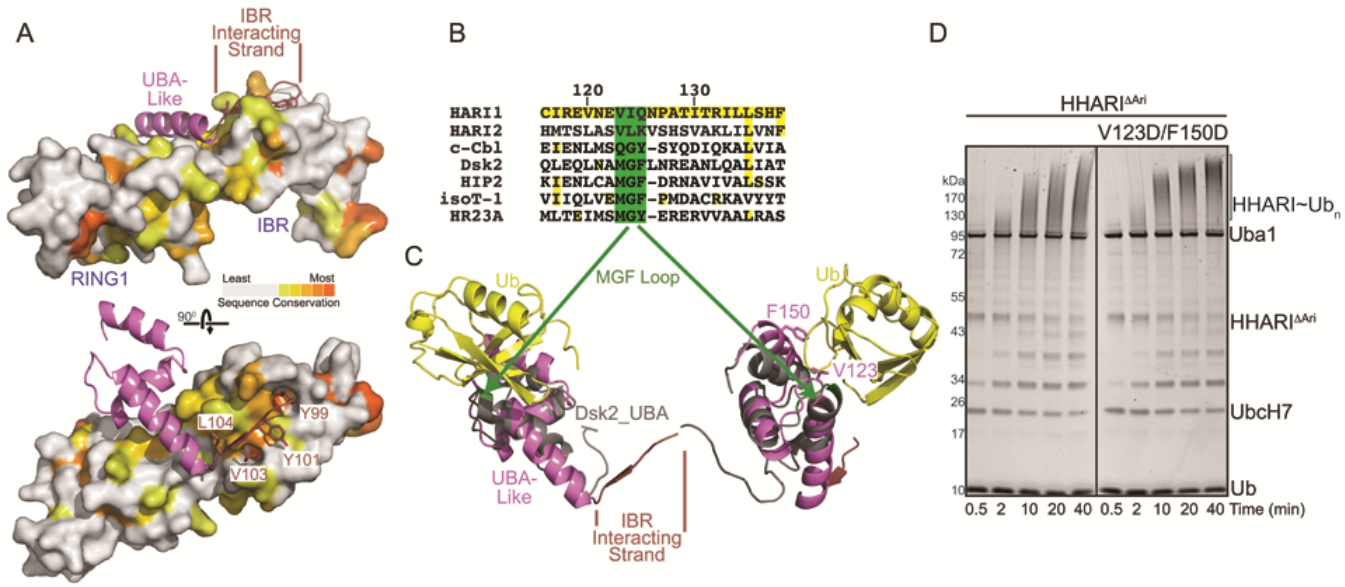


**Figure S4. Analysis of HHARI UBA-like domain. [supports Figure 5]**

A. Space filling model of HHARI RING1 and IBR domains with sequence conservation over Ariadne family members displayed as white (low homology) to orange (high homology). The HHARI UBA-like domain and IBR-interacting-strand region (with important IBR contacting residues shown) are represented as cartoons.

B. Sequence alignment of HHARI (HARI1) and HARI2 UBA-like domains with known ubiquitin-interacting UBA domains from c-Cbl, Dsk2, HIP2, isoT-1, and HR23A. The MGF loop that in these latter UBA domains is important for ubiquitin-binding is highlighted in green.

C. Structure of HHARI UBA-like domain superimposed on the structure of Dsk2 UBA in complex with ubiquitin (Ohno et al., 2005). The position of the MGF loop is colored green.

D. Based on the superimposed structure of Dsk2-Ubiquitin, mutations were made in the HHARI UBA-like domain (V123D, which corresponds to the position of the Dsk2 methionine in the MGF loop, and F150D) that would be predicted to disrupt UBA domain-ubiquitin interactions. These mutations do not have an obvious effect on HHARIΔAriadne-mediated polyubiquitination.

**Table S1. Selected contacts between HHARI RING2 and Ariadne domains. [supports Figure 4]**

| RING2 | | Ariadne Domain | |
|---|---|---|---|
| Ala | 339 | Gln | 426 |
| Lys | 353 | Phe | 430 |
| | | Gln | 426 |
| Asp | 354 | Phe | 430 |
| Gly | 355 | Phe | 430 |
| | | Glu | 510 |
| Gly | 356 | Ser | 506 |
| | | Ser | 427 |
| | | Glu | 431 |
| | | Glu | 510 |
| | | Phe | 430 |
| Cys | 357 | Ser | 506 |
| | | Glu | 431 |
| | | Glu | 510 |
| | | Glu | 503 |
| | | Gly | 507 |
| Asn | 358 | Glu | 503 |
| | | Asn | 423 |
| | | Ser | 427 |
| | | Glu | 503 |
| His | 359 | Arg | 511 |
| Trp | 373 | Asn | 423 |
| Val | 374 | Arg | 420 |
| | | Asn | 419 |
| | | Asn | 423 |
| Trp | 379 | Glu | 503 |
| Cys | 389 | Phe | 416 |
| | | Arg | 420 |
| Asn | 390 | Phe | 416 |
| | | Tyr | 476 |
| | | Gln | 495 |
| | | Ala | 496 |
| | | Glu | 492 |
| Arg | 391 | Phe | 416 |
| Tyr | 392 | Phe | 416 |

SUPPLEMENTARY EXPERIMENTAL PROCEDURES

**Protein expression and purification**

All proteins described correspond to human sequences. HHARI was cloned in frame with GST in pGEX4T1 (GE) modified to contain a TEV proteolytic cleavage site (pGEX4T1-TEV). HHARI was purified by glutathione affinity chromatography, followed by TEV proteolysis to liberate GST, and anion exchange and size exclusion chromatography in 20 mM Tris-HCl, 100 mM NaCl, 1 mM DTT, concentrated, aliquotted, flash-frozen, and stored at -80 $^{o}$C. UBA1, UbcH7, and ubiquitin used in biochemical and biophysical experiments were prepared as described (Duda et al., 2012; Huang et al., 2008).

**Analytical Ultracentrifugation and SEC-MALS**

The sedimentation velocity analytical ultracentrifugation (SV-AUC) experiment was conducted in a ProteomeLab XL-I analytical ultracentrifuge (Beckman Coulter, Fullerton, CA) with protein at 1 mg/mL in 25 mM HEPES pH 7.6, 100 mM NaCl and 1 mM DTT buffer following standard protocol (Brown et al., 2008). A loading volume of 350 µl buffer and protein sample were placed in the reference and sample sectors of the Epon double-sector centerpiece sandwiched between two sapphire windows. The cell assembly was placed in a four hole An60-Ti rotor, temperature equilibrated in the centrifuge to a nominal temperature of 20 °C and then evenly accelerated to 50,000 rpm. Fringe displacement data at time intervals of 1.0 min were collected with the Rayleigh interference system for 12 hours and analysed in SEDFIT (https://sedfitsedphat.nibib.nih.gov/software) using the model for continuous sedimentation coefficient distribution *c(s)* with deconvolution of diffusional effects (Schuck, 2000). The sedimentation coefficient distribution *c(s)* was calculated with maximum entropy regularization at a confidence level of p = 0.68 and at a resolution of sedimentation coefficients of n = 100. The positions of the meniscus and bottom, as well as time-invariant and radial noises, were fitted.

The size-exclusion chromatography multi-angle light scattering (SEC-MALS) experiment was carried out by using a Shodex PROTEIN KW-803 (exclusion limit 150,000 Da) size-exclusion column (SHOWA DENKO, Kanagawa, Japan) with three detectors connected in series: an Agilent 1200 ultraviolet (UV) detector (Agilent Technologies, Santa Clara, CA), a Wyatt DAWN-HELEOS multi-angle light-scattering (MALS) and a Wyatt Optilab rEX differential refractive index (RI) detector (Wyatt Technologies, Santa Barbara, CA, USA). The column was equilibrated with 25 mM HEPES pH 7.6, 100mM NaCl and 1 mM DTT buffer, and the experiment was conducted at 25 °C. A volume of 25 µL of a 0.8 mg/ml sample in buffer was placed on the column with the auto-sampler, and a flow rate of 0.4 ml/min was maintained throughout the experiment. Protein in the eluent was detected and measured via light scattering and absorbance at 280 nm, and the data were recorded and analyzed with the Wyatt Astra software (version 6.0.5.3). EASI Graphs (Astra software) were exported and plotted as a molar mass distribution superimposed on a chromatogram of absorbance at 280 nm versus elution volume (Kendrick et al., 2001).

SUPPLEMENTARY REFERENCES

Brown, P.H., Balbo, A., and Schuck, P. (2008). Characterizing protein-protein interactions by sedimentation velocity analytical ultracentrifugation. Current protocols in immunology / edited by John E Coligan [et al] *Chapter 18*, Unit 18 15.

Duda, D.M., Olszewski, J.L., Tron, A.E., Hammel, M., Lambert, L.J., Waddell, M.B., Mittag, T., DeCaprio, J.A., and Schulman, B.A. (2012). Structure of a glomulin-RBX1-CUL1 complex: inhibition of a RING E3 ligase through masking of its E2-binding surface. Molecular cell *47*, 371-382.

Huang, D.T., Zhuang, M., Ayrault, O., and Schulman, B.A. (2008). Identification of conjugation specificity determinants unmasks vestigial preference for ubiquitin within the NEDD8 E2. Nature structural & molecular biology *15*, 280-287.

Kendrick, B.S., Kerwin, B.A., Chang, B.S., and Philo, J.S. (2001). Online size-exclusion high-performance liquid chromatography light scattering and differential refractometry methods to determine degree of polymer conjugation to proteins and protein-protein or protein-ligand association states. Anal Biochem *299*, 136-146.

Ohno, A., Jee, J., Fujiwara, K., Tenno, T., Goda, N., Tochio, H., Kobayashi, H., Hiroaki, H., and Shirakawa, M. (2005). Structure of the UBA domain of Dsk2p in complex with ubiquitin molecular determinants for ubiquitin recognition. Structure *13*, 521-532.

Schuck, P. (2000). Size-distribution analysis of macromolecules by sedimentation velocity ultracentrifugation and lamm equation modeling. Biophys J *78*, 1606-1619.